Published in final edited form as:

Cell Rep. 2022 September 27; 40(13): 111432. doi:10.1016/j.celrep.2022.111432.

Cell-type identity of the avian utricle

Mirko Scheibinger[1,2,3,*], **Amanda Janesick**[1,2,3], **Nesrine Benkafadar**[1,2], **Daniel C. Ellwanger**[1,2,5], **Taha A. Jan**[1,4], **Stefan Heller**[1,2,6,*]

[1]Department of Otolaryngology–Head and Neck Surgery, Stanford University School of Medicine, Stanford, CA 94305, USA

[2]Institute for Stem Cell Biology and Regenerative Medicine, Stanford University School of Medicine, Stanford, CA 94305, USA

[3]Present address: 10X Genomics, Pleasanton, CA 94588, USA

[4]Present address: Department of Otolaryngology-Head and Neck Surgery, Vanderbilt University Medical Center, Nashville, TN 37232, USA

[5]Present address: Genome Analysis Unit, Amgen Research, Amgen Inc., South San Francisco, CA 94080, USA

[6]Lead contact

SUMMARY

The avian utricle, a vestibular organ of the inner ear, displays turnover of sensory hair cells throughout life. This is in sharp contrast to the mammalian utricle, which shows limited regenerative capacity. Here, we use single-cell RNA sequencing to identify distinct marker genes for the different sensory hair cell subtypes of the chicken utricle, which we validated *in situ*. We provide markers for spatially distinct supporting cell populations and identify two transitional cell populations of dedifferentiating supporting cells and developing hair cells. Trajectory reconstruction resulted in an inventory of gene expression dynamics of natural hair cell generation in the avian utricle.

Graphical abstract

[*]Correspondence: mscheib@stanford.edu (M.S.), hellers@stanford.edu (S.H.).

AUTHOR CONTRIBUTIONS

Conceptualization: M.S. and S.H.; methodology: M.S., A.J., D.C.E., and T.A.J.; formal analysis: M.S. and D.C.E.; investigation: M.S., A.J., and N.B.; resources: M.S., D.C.E., and T.A.J.; writing – original draft: M.S. and S.H.; writing – review & editing: M.S. and S.H.; visualization: M.S., N.B., and T.A.J.; supervision: M.S. and S.H.; funding acquisition: A.J., N.B., and S.H.

SUPPLEMENTAL INFORMATION

Supplemental information can be found online at https://doi.org/10.1016/j.celrep.2022.111432.

DECLARATION OF INTERESTS

S.H. is a paid consultant of Pipeline Therapeutics and Lineage Cell Therapeutics.

INCLUSION AND DIVERSITY

We support inclusive, diverse, and equitable conduct of research.

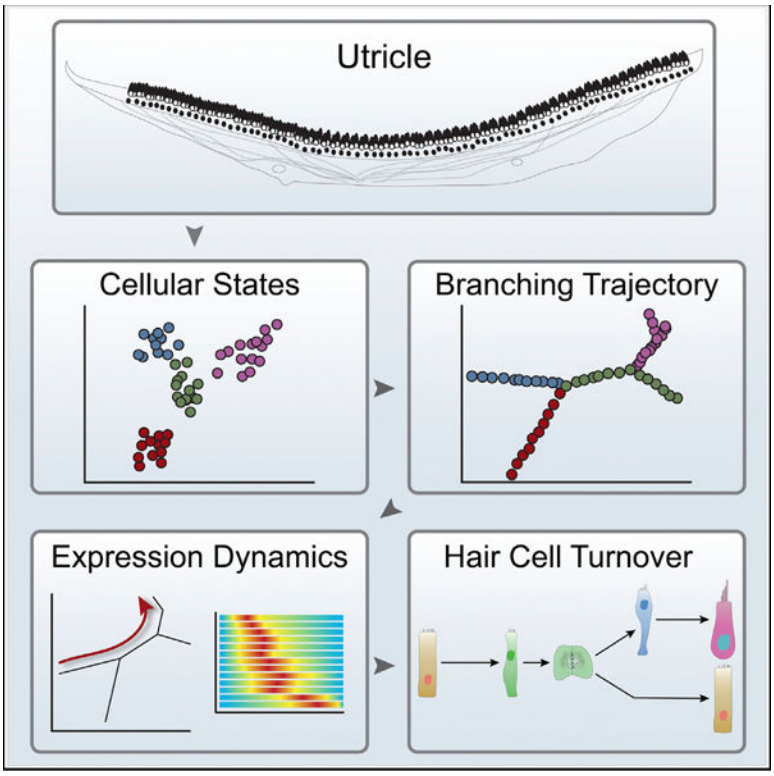

In brief

Scheibinger et al. provide a single-cell transcriptomic atlas of the chicken utricle, a vestibular organ. Hair cell and supporting cell subtypes are defined by marker genes, and trajectories of gene expression dynamics during hair cell turnover are shown. This resource provides a baseline to study inner ear damage and regeneration.

INTRODUCTION

The utricle is a sensory organ of the vestibular apparatus that detects linear accelerations. It harbors a sensory epithelium, the macula, consisting of mechanosensitive hair cells and associated supporting cells. The macula comprises an elongated striola surrounded by regions of extrastriolar sensory epithelium facing the midline and the side of the head, known as medial extrastriola and lateral extrastriola. Within the striola is the line of polarity reversal, where the polarity of sensory hair cells and their hair bundles change (Figures 1A, 1B, and S1A).

Over 60 years ago, Wersäll described two types of vestibular hair cells in amniotes (Wersall, 1956): flask-shaped type I hair cells innervated by afferent nerve calyces and the cylindrical type II hair cells that form synapses with both afferent and efferent bouton terminals. In birds and reptiles, the extrastriolar regions are exclusively composed of type II hair cells contacted by synaptic boutons (Warchol and Speck, 2007). The striola features type I hair cells innervated by calyces and a subtype of type II hair cells located along the line of polarity reversal (Warchol and Montcouquiol, 2010). In mammals, type I hair cells occur

in both striolar and extrastriolar regions. Hair cells in the avian striola have shorter hair bundles with thicker stereocilia compared with extrastriolar hair cells that display long hair bundles with thin stereocilia. Supporting cells interdigitate hair cells throughout the striolar and extrastriolar regions. Whereas the expression of multiple marker genes defines utricular type I and type II hair cells, only a few markers are known for supporting cell subgroups (Burns et al., 2015).

Non-mammalian vertebrates naturally turn over utricle hair cells throughout life (Goodyear et al., 1999). This happens via the mitotic division of supporting cells located near the lost hair cells and subsequent differentiation into new hair cells and supporting cells. Non-mammalian supporting cells are facultative stem cells, and hair cell regeneration, consequently, happens naturally in the avian utricle (Janesick and Heller, 2019). In contrast, mammalian utricle supporting cells lose the ability of mitotic hair cell replacement during the first postnatal week (Burns et al., 2012a).

Our goal was to assemble a detailed molecular map of the mature chicken utricle using single-cell RNA sequencing (scRNA-seq). In addition to identifying distinct marker genes for different cell types, we hypothesized that we would be able to capture dynamic changes in gene expression during the natural generation of new hair cells. Toward these goals, we conducted transcriptomic profiling of chicken utricle cells at post-hatch day 7 (P7), when the avian inner ear is fully functional. We detected a median of 2,700 genes per individual cell, allowing the construction of a spatial map representing striolar and extrastriolar cell groups. *In situ* validation confirmed mRNA expression of markers for all subtypes of utricle hair cells and supporting cells. We define three types of hair cells: extrastriolar type II, striolar type I, and striolar type II. A population of distinct supporting cells was notable along the line of cell polarity reversal. No gene expression differences were noted in other supporting cells associated with general striolar and extrastriolar regions. Moreover, we extracted a temporal trajectory representing the de-differentiation of supporting cells into progenitor cells that give rise to new hair cells. We propose a sequence of dynamic changes in gene expression associated with supporting cells as they engage in new cell production, followed by the emergence of nascent hair cells that differentiate into the different hair cell subtypes. Our data provide an in-depth transcriptomic inventory of all cell types of the chicken utricle as a resource for the neuroscience and regenerative biology communities.

RESULTS

Transcriptional profiling of P7 chicken utricle sensory epithelium cells

To investigate cellular heterogeneity and new cell production in the utricle, we collected viable sensory epithelial cells using fluorescence-activated cell sorting (FACS) (Figure 1C). We sequenced 379 libraries from selected high-quality cDNA preparations at a depth of ≈1 million 150 bp reads per cell. The raw reads were aligned to the NCBI *Gallus gallus* v6.0 reference genome and were mapped to protein-coding genes. Fifty-seven information-poor cells and 3,952 low-abundant genes were removed. The resulting raw count matrix of 322 cells and 13,643 genes was normalized using SCnorm (Bacher et al., 2017) and analyzed with CellTrails (Ellwanger et al., 2018).

CellTrails utilized the lower-dimensional manifold of a submatrix of the 323 most variable genes in the dataset to identify a latent spatiotemporal data structure consisting of eight distinct cellular subgroups (states, S1–S8) (Figure 1D). Cells in S1–S3 express known supporting cell genes such as *AGR3* (Zhu et al., 2019) and lack expression of hair cell markers such as *OTOF* (Goodyear et al., 2010) (Figure 1E). Reciprocally, states S5–S8 consist of hair cells exemplified by high levels of *OTOF* and the absence of *AGR3*. The main features of S4 cells are genes associated with non-sensory epithelium cells (Figures S1B–S1D and Table S1A). Our decision to remove S4 cells from subsequent analyses was further supported when we used CellTrails to construct an ordered trajectory, which did not identify reasonable concordances of the S4 group with any other cell group. The remaining supporting cell (S1–S3) and hair cell groups (S5–S8) were aligned onto a branching trajectory (Figure 1F). We conclude that the P7 utricle sensory epithelium consists of a heterogeneous population of supporting cells and hair cells. The cells were ordered along a trajectory guided by spatial and temporal factors, comparable to the trajectories reported in recent single-cell transcriptomic and proteomic analyses of the developing chicken utricle (Ellwanger et al., 2018; Zhu et al., 2019). We focused our subsequent investigations on revealing spatial and temporal gene expression patterns.

Markers for hair cells and supporting cells

Differential gene expression analysis between the combined supporting cell groups S1–S3 and the combined hair cells S5–S8 revealed 201 genes distinctively enriched in the supporting cell group and 1,129 genes associated with hair cells at a false discovery rate (FDR) < 0.01 and $\log_2$-fold change > 2 (Figures 2A, 2B, and 2E and Table S1A). We identified known supporting cell genes such as *AGR3*, *GJB2*, *GJB6*, *SPARC*, *TMSB4X,* and *OTOGL* and found previously unknown utricular supporting cell-specific genes like *ADGRG6* and *ZBTB20*. Conversely, known hair cell-specific genes such as *STARD10*, *OTOF*, and *GPX2* were accompanied by additional marker genes for utricular hair cells such as *C4H4ORF50*, *LOC419602*, *SYT14*, *B3GNTL,* and *SCG3* (Figure 2B). We validated marker genes identified with differential gene expression analysis by *in situ* hybridization. Transcripts for *ZBTB20* and *GJB6* were confirmed to be high in supporting cells compared with surrounding hair cells (Figure 2C). We noticed that the mRNA of some genes was asymmetrically distributed in the cytoplasm of supporting cells, such as the restriction of *MATN4* and *ZBTB20* to the apical and basal compartments, respectively (Figure S2). The subcellular localization of mRNA is a known biologically significant feature of various cell types (Martin and Ephrussi, 2009) but has not been systematically studied in the inner ear, where it has recently been noted (Janesick et al., 2021). Expression of *GPX2*, *CALB2*, *C4H4ORF50*, *B3GNTL*, and *SYT14* mRNA was confirmed in hair cells (Figures 2D and S2B).

Hair cell diversity

To explore the distinct differences among the four hair cell groups S5–S8, we performed differential gene expression analyses between each group and all remaining cells. Our goal was to identify specific marker genes for each hair cell group, assign group identities, and obtain candidate genes for detecting the corresponding cells in the utricle *in situ*. For cell group S5, we identified 361 genes that were significantly enriched (Figures 3A and 3B

and Table S1A). High expression of previously defined extrastriolar markers *OSBPL1A*, *CAB39L*, and *SYN3* (Ellwanger et al., 2018) suggest that S5 represents extrastriolar type II hair cells. We also identified other presumptive extrastriolar hair cell markers such as *GRAMD3*, *CABP1*, and *RASD2*. *RASD2* has previously been described in immature mouse utricle hair cells (Burns et al., 2015). The identity of S5 was confirmed by *in situ* detection of mRNA for *GRAMD3*, *CABP1*, and *RASD2* in extrastriolar type II hair cells (Figures 3C, S3A, and S4A).

Comparing the hair cell group S8 with all remaining cells showed enrichment of 356 genes (Figure 3B and Table S1A). Using *in situ* hybridization, we confirmed the expression of the identified S8 markers *KCNQ5*, *RPP25*, *LTK*, and *SYT12*, distinctively in striolar type I hair cells (Figures 3D, S3A, and S3B).

Having identified the chicken utricle's two primary hair cell groups, extrastriolar type II (S5) and striolar type I hair cells (S8), we were curious about the identity of the two remaining clusters S6 and S7. Seventy-two genes were differentially expressed in S7, including *C14ORF180*, *TNNC2*, *S100Z*, and *TMC2* (Figures 3B, 3E, and S4 and Table S1A). Whereas *TMC2* expression was high in all striolar hair cells, *C14ORF180*, *TNNC2*, and *S100Z* expression was detected in a subset of the striolar hair cells (Figures 3E and S4), specifically located near the line of polarity reversal (LPR), where striolar type II hair cells have been previously reported (Jorgensen, 1989; Warchol and Speck, 2007). Therefore, we conclude that S7 cells represent striolar type II hair cells defined by a distinct subset of genes (Table S1A).

Finally, we compared cluster S6 with all other sensory epithelium cells and noted 521 distinct genes (Figure 3B and Table S1A). *ATOH1*, an essential gene for hair cell differentiation (Bermingham, 1999), is prominently expressed in S6, suggesting that this group represents differentiating cells that transition toward hair cells. Several genes, such as *LOC107053413*, *HTR3A*, *NHLH1*, *GNG13*, *NREP* (Hawkins et al., 2006), and *LINGO3*, were distinctively expressed in S6. We detected dispersed *ATOH1*, *LINGO3*, and *NREP* mRNA expression across the utricle sensory epithelium, supporting our hypothesis that S6 represents differentiating and nascent hair cells (Figure 3F). We conclude that our analysis and the *in situ* validation of the hair cell groups S5, S8, and S7 revealed extrastriolar type II, striolar type I, and striolar type II hair cells, respectively. S6 represents transitional cells that express *ATOH1* and an assortment of additional, previously unknown, nascent hair cell markers.

Heterogeneity of supporting cells

Differential gene expression analysis of the supporting cell clusters identified 137 genes significantly enriched in S1, including the known supporting cell genes *OTOL1*, *SLC1A3*, *DKK3*, *MATN4*, and *SPARC*, as well as previously unknown genes such as *SERPINF2* (Figures 4A and 4B and Table S1A). Validation of *OTOL1* mRNA revealed intense labeling of all supporting cells, except for a subgroup of supporting cells associated with the central striolar region (Figure 4C). We conclude that S1 represents a general chicken utricle supporting cell type.

A comparison of S2 to all remaining cells revealed 261 significantly enriched genes (Figures 4B and 4D and Table S1A). Known supporting cell genes *OTOA* and *SOX10* but also additional genes such as *IGFBP7*, *HS3ST1*, LOC419390, *FAM69C*, and *SMOC2* were associated with S2. Validation of S2-enriched genes revealed *GATA3*, *TECTB*, and *SMOC2* mRNA expression in striolar supporting cells along the LPR; antibodies to GATA3 labeled the nuclei of S2 cells associated with the reversal zone (Figures 4D and S5). The transcription factor GATA3 and TECTB, a secreted component of the otolithic membrane, are markers of supporting cells associated with the LPR (Warchol and Speck, 2007) (Figures S6A and S6B). Forty-one supporting cells and 36 striolar type II hair cells in S7 co-expressed *GATA3* and *TECTB* (Figures S6C–S6E). We identified and visualized *GATA3*/*TECTB* double-positive cells and noticed that they were distributed along the striolar-supporting-cell-to-striolar-type-II-hair-cell trajectory that includes S2, S3, S6, and S7. (Figure S6C). *GATA3*/*TECTB* double-positive cells define a subset of striolar supporting cells. Comparison of *GATA3*/*TECTB* double-positive supporting cells with all remaining supporting cells revealed a statistically significant enrichment of 42 genes. Known striolar markers such as *TECTB* and *GATA3* and additional markers like *SPON1*, *COX11*, and *WDR37* were associated with this subset (Figure S6D and Table S1A). When we compared *GATA3*/*TECTB* double-positive hair cells to all remaining hair cells from S6–S8, we identified 34 significantly enriched genes (Figure S6E and Table S1A). The top genes were *GXYLT2*, *FZD10*, *GATA3*, *CCNY*, and *IFI30*.

Fifty-eight genes were distinctively expressed in S3, including many previously unknown supporting cell genes: *LRRN4*, *CHST15*, *RARRES2*, *C4A*, *NINJ2*, and *GADD45B* (Figures 4B and 4E and Table S1A). Notably, S3 cells were located along the trajectory between the main two supporting cell branches and the nascent hair cell group S6 (Figure 1F). Based on this distinctive trajectory position, we hypothesized that S3 cells represent dedifferentiating supporting cells that might contribute to new hair cell production and turnover. We decided to focus on the two putative transitional groups S3 and S6.

Transitional supporting cells and emerging hair cells

A comparison of the two transitional cell groups S3 and S6 revealed 81 and 1,062 significantly enriched genes associated with S3 and S6, respectively (Figures 5A–5C). Supporting cell markers such as *SPARC*, *SOX10*, *GJB6*, *FADS2*, and *S100A6* suggest that S3 cells are related to supporting cells. Several top differentially expressed genes in S6 are known hair cell genes, such as *GPX2*, *LHX3*, *CXCL14*, *OAZ1* (Ranum et al., 2019), and *CALB2* (Figure 5B). Based on this comparison, we hypothesize that cells in S3 are derived from supporting cells, and S6 cells represent a population of emerging hair cells. We were curious about what distinguished S3 from the supporting cells and compared S3 with S1 and S2. We identified nine significantly enriched genes, of which five specifically differentiate S3 cells from supporting cells: *IRF7*, *PMP22*, *B3GAT1L*, *MYC*, and *CALM2* (Figures 5D–5F). The other four genes, *GADD45B*, *LRRN4*, *MAFF*, and *DDIT3*, were already identified as S3 specific compared with all cells (Figures 4B and 4E). Twenty-seven genes, mainly known supporting cell markers (*SLC1A3*, *OTOL1*, *DKK3*, *JAG1*, *TECTA*), are significantly lower expressed in S3 cells when compared with S1 and S2, suggesting that the S3 cells are in the process of losing specific supporting cell marker expression, some exceeding 30-fold

reduction (Figure 5E). This downregulation can be appreciated when the gene expression levels for *SLC1A3*, *OTOL1*, *DKK3*, and *JAG1* are projected on the CellTrails trajectory map (Figure 6A).

When we compared S6 with all remaining hair cells (S5, S7, S8), 212 genes were significantly enriched (Figures 5G and 5H). One hundred seventy-six of these genes were among the 521 genes previously identified (Figure 3B and Table S1A) as differentially expressed in S6 compared with all cell groups, which provided the basis for describing this cell group as emerging hair cells. While 36 distinct genes discriminated S6 from the more differentiated hair cells, we noticed several genes that were also expressed in supporting cells, such as *COL9A1*, *TMSB4X*, *ADGRG6*, *ZBTB20, EPCAM*, and *ACTB* (Figures 5H–5J). We recently identified *TMSB4X* as a gene that is downregulated to allow the commencement of hair bundle assembly, whereas *EPCAM* expression is lower in hair cells compared with supporting cells (Zhu et al., 2019). The gene expression pattern of S6, therefore, suggests that these cells have adopted a nascent hair cell phenotype, still expressing a few supporting cell genes, and they have not started with the assembly of hair bundles.

We next sought to identify S6 cells *in situ* in the utricle sensory epithelium. Presuming that new hair cells differentiate after supporting cell division, we injected chickens with 5-ethynyl-2'-deoxyuridine (EdU) and identified cells that incorporated EdU during S-phase after 24 h. We found cells with EdU-positive nuclei within the supporting cell layer of the utricle (Figure 6B). Most EdU-positive cells occurred in pairs, confirming that homeostatic hair cell generation in the chicken utricle happens exclusively through asymmetric supporting cell division (Scheibinger et al., 2018). Co-labeling for *ATOH1* mRNA revealed pairs of EdU-positive cells where one cell expresses *ATOH1*, and the sister cell does not (Figure 6C). We found asymmetric *ATOH1* mRNA expression in EdU-positive pairs in the extrastriolar and striolar regions. This finding identifies the *ATOH1* expressing EdU-positive cells as S6 nascent hair cells. Conversely, the *ATOH1*-negative EdU-positive sister cells are en route toward becoming supporting cells. Computationally, a loopback of the newly generated cells that do not differentiate into hair cells toward supporting cells is challenging to resolve. One could suppose that a returning transitional cell to the supporting cell phenotype looks transcriptionally similar to dedifferentiation, and the return path is consequently happening in reverse along the S3 trajectory (Figure 6D). Detecting subtle gene expression differences along this return path might require sampling more transitional cells, which could be a limitation of our method.

Biological pathways in the P7 utricle

To gain mechanistic insight into gene lists obtained from differential gene expression analyses for all cell groups, we performed pathway enrichment analysis using g:Profiler (Raudvere et al., 2019) and visualized results with Cytoscape (Shannon et al., 2003). Gene enrichment terms associated with supporting cell groups S1 and S2 included processes such as ''regulation of signaling'' (S2), ''cell adhesion'' (S1), and ''regulation of peptidase activity'' (S1). Interestingly, our pathway enrichment analysis identified cell proliferation associations in all supporting cell groups (S1–S3). For example, S1 and S2 genes were

enriched in processes related to ‘‘cell population proliferation,’’ whereas genes shared by all supporting cell groups were associated with gene ontology (GO) processes such as ‘‘tissue development’’ (Figure S7A and Tables S1B and S1C).

Supporting cells from S3 were associated with the p38 mitogen-activated protein kinases pathway involved in orchestrating proliferation (Wagner and Nebreda, 2009). Most genes from the nascent hair cell group S6 were significantly enriched in GO processes ‘‘hair cell differentiation’’ and ‘‘microtubule bundle formation.’’ In extrastriolar type II hair cells from S5, we identified ‘‘neuron differentiation,’’ ‘‘synaptic vesicle cycle,’’ and ‘‘cation transmembrane transport.’’ Ion channels were associated in striolar type I (S8) and type II (S7) hair cells through GO processes such as ‘‘voltage-gated potassium channels’’ and ‘‘sodium ion transmembrane transport.’’ Pathway enrichment analysis fits with our reconstructed bifurcating P7 utricle single-cell trajectory that spans from supporting cells (S1–S2) via transitional supporting (S3) and hair cells (S6) to mature extrastriolar (S5) and striolar (S7–S8) hair cells (Figure S7A and Tables S1B and S1C).

To evaluate cell cycle processes in more detail in dedifferentiating supporting cells (S3) and nascent hair cells (S6), we investigated cell cycle process gene expression (GO: 0022402, 1,152 genes) in our dataset. Among the 565 expressed cell cycle process genes across all states, 44 genes were associated with supporting cells from S3 (cluster 1) and 295 genes with nascent hair cells from S6 (Figure S7B, and Table S1C). Pathway enrichment analysis using these two gene lists revealed two significantly enriched GO biological processes and Reactome pathways for S3 and 43 for S6 (Figure S7C and Table S1C). GO processes such as ‘‘cell cycle G1/S-phase transition’’ and ‘‘G1/S transition of mitotic cell cycle’’ were significantly enriched in supporting cells from S3. Also, cell cycle processes were associated with nascent hair cells from S6 with significant enrichment of GO processes such as ‘‘M phase,’’ ‘‘regulation of cell cycle,’’ and ‘‘cell cycle process’’ (Figure S7C and Table S1C).

Gene expression dynamics in the P7 utricle

After giving each state a cellular identity, we assessed gene expression dynamics along a trajectory from supporting cells (S1, S2), via transitional supporting cells (S3), nascent hair cells (S6), toward extrastriolar type II hair cells (S5) (Figure 7A). Among the differentially expressed genes from these cell groups, we found 1,404 genes that dynamically changed expression along the path from extrastriolar supporting cells toward type II hair cells. For example, the expression of the supporting cell marker *SPARC* decreases, whereas *GRAMD3*, an extrastriolar type II hair cell marker (S5), increases as pseudotime progresses (Figure 7B). *ATOH1*, an S6 nascent hair cell marker, peaks between *SPARC* and *GRAMD3* and is downregulated toward the end of the pseudotime axis. *SOX10*, a marker for the transitional supporting cells in S3, peaks before *ATOH1* and is turned off when *ATOH1* peaks. In contrast to general supporting cell markers, reversal zone marker genes such as the striolar type II hair cell marker *C14ORF180* and the type I hair cell marker *KCNQ5* were not significantly expressed along the extrastriolar pseudotime axis (Figure 7B). Gene expression dynamics clustered into four significantly different groups (Figure 7C and Table S2). Cluster 1 consists of 150 genes that peaked early and decreased along the pseudotime axis. We found S1 supporting cell genes such as *SPARC*, *OTOL1*, *SLC1A3*, *MATN4*, *GJB2*,

and *SOX10* from S3 in cluster 1. Cluster 2 harbors 489 gene expression dynamics that peak around the midpoint and are downregulated toward the end of the trajectory. Cluster 3 represents 749 gene expression dynamics that are turned on halfway along the trajectory. Genes found in cluster 3 are extrastriolar hair cell markers such as *CABP1*, *GRAMD3*, and *CAB39L*. Gene expression dynamics (19 genes, *PRSS35*, *LGMN*, *CLSTN1*) in cluster 4 are on early, off at midpoint, and turned on again when *ATOH1* peaks.

Next, we examined transcription factor gene expression dynamics. One hundred sixteen transcription factors clustered into five significantly different groups. We identified transcription factors that peak early (cluster 1; 19 genes), pre-*ATOH1* (cluster 2; 18 genes), with *ATOH1* at the midpoint (cluster 3; 10 genes), at the midpoint but stayed on (cluster 4; 59 genes), and at the trajectory's end (cluster 5; 10 genes). Using 53 orthologs of human deafness genes, we identified four clusters comprised of an early group, genes that transiently peak at the midpoint, genes turned on at the midpoint, and genes that peak late (Figure 7C and Table S2).

We next inferred gene expression dynamics from the supporting cells toward type I hair cells, which are exclusively located in the striola (Figure 7D). Because the initial half of this trajectory is the same as the extrastriolar type II trajectory, we did not note substantial differences until after the ATOH1 peak, when type I marker genes (i.e., *KCNQ5*) were strongly upregulated (Figure 7E). We identified four significantly different groups of dynamically regulated genes (Figure 7F and Table S3). Clusters 1 and 2 were highly similar to the equivalent clusters in the type II trajectory, representing downregulation of supporting cell genes and genes that are active during early hair cell differentiation, including *ATOH1* and *LINGO3*. For transcription factors, we made three observations. First, a group of transcription factors were upregulated toward the end of the extrastriolar type II and the striolar type I trajectory: *GFI1*, *LHX3*, *CARHSP1*, *IRX2*, and *THAP4*, among others. Second, we identified transcription factors specifically upregulated along the type I-specific hair cell differentiation (*ISL1*, *IKZF2*). Finally, transcription factor cluster 5 of the type II trajectory (Figure 7C) represents candidates that are specifically upregulated when extrastriolar type II hair cells differentiate and include *ARNT*, *CREB5*, *ESRRG*, *TUB*, and *ZNF827*. We noted that *INSM1* expression is associated with the nascent hair cell cluster, *TBX2* is expressed en route toward striolar hair cell subtypes, and *IKZF2* in maturing striolar hair cells (Table S1D). These transcription regulators are involved in specifying the two mammalian cochlear hair cell subtypes (Chessum et al., 2018; Garcia-Anoveros et al., 2022; Wiwatpanit et al., 2018). As in the extrastriolar type II trajectory, we found 51 deafness gene expression dynamics that are clustered into four groups (Figure 7F and Table S3).

DISCUSSION

For decades, the avian inner ear has provided a prospect for the development of hearing loss therapies. In sharp contrast to mammals, the cochlear and vestibular sensory epithelia of birds naturally and functionally recover from hair cell loss. Although the cytomorphological changes during hair cell regeneration are well described, the mechanisms underlying the coordinated sequence of activation or inhibition of signaling pathways are not sufficiently

understood. Our analysis provides a baseline for comparative studies aimed at unraveling the mechanisms of avian hair cell regeneration.

Unsupervised clustering, differential gene expression analysis, and *in situ* validation allowed us to discriminate between distinct subpopulations of supporting cells and hair cells. Moreover, we used single-cell gene expression data to resolve transient cellular states during natural hair cell generation. We surmise that natural turnover is distinct from hair cell regeneration, which elevates our analysis to an essential data collection to discriminate hair cell regenerative pathways.

Hair cells

We identified three subtypes of mature vestibular hair cells, and our marker gene validation confirmed that extrastriolar regions of the chicken utricle macula harbor exclusively type II hair cells. Type I hair cells occupy the striola, and a second type II subtype of hair cells is located along the LPR. This observation agrees with known hair cell subtype distribution (Warchol and Montcouquiol, 2010; Warchol and Speck, 2007). Notably, we found that the mechanoelectrical transduction channel component *TMC1* is expressed in all hair cells, but *TMC2* and *CIB2*, a proposed linker between the mechanoelectrical transduction channel and the actin cytoskeleton (Giese et al., 2017), were only detected in striolar type I and striolar type II hair cells. Cell-type-specific gene expression and expression dynamics of genes mentioned in the discussion are shown in Table S1D.

Our data show that chicken vestibular hair cells express the RIBEYE protein-encoding gene *CTBP2* and other ribbon-associated genes such as *CTBP1*, *PCLO* (Piccolo), *KIF3A*, *UNC119B*, *RIMS1*, and *BSN* (Bassoon). The active zone compartment of ribbon synapses includes genes such as *RIMS2*, *ERC1*, *ERC2*, and *CACNA1D* (Cav1.3). All these genes were expressed by all hair cells except for *RIMS2*, which was restricted to extrastriolar type II hair cells. In addition, we identified two syntaxins (*STX1A*, *STX12*), *SNAP25*, and several vesicle-associated membrane protein (*VAMP*) genes to be expressed in hair cells. *VAMP2* was highly enriched in extrastriolar type II hair cells, as well as *SNAP91*, encoding the AP180 protein involved in synaptic vesicle recycling.

OTOF is the principal calcium sensor in hair cell exocytosis. We found *OTOF* expression and confirmed the lack of *SYT1* and *SYT2* in vestibular hair cells (Beurg et al., 2010). Nevertheless, we identified *SYT14*, a presumed Ca^{2+}-independent synaptotagmin (Fukuda, 2003), in all hair cells, and *SYT12* specifically in striolar type I hair cells. Chicken auditory hair cells do not express synapsins 1 and 2 (*SYN1*, *SYN2*) (Uthaiah and Hudspeth, 2010). Both genes were also not detectable in vestibular hair cells, but we found *SYN3* expression in all hair cells. In agreement with other reports (Safieddine and Wenthold, 1999; Strenzke et al., 2009; Uthaiah and Hudspeth, 2010), we did not observe expression of synaptophysins and complexins.

Although the electrophysiological properties of potassium conductances in vestibular type I and type II hair cells are well understood, information about the molecular nature of these potassium channels is incomplete (Eatock, 2018; Meredith and Rennie, 2016). We found *KCNQ5* specifically in striolar type I hair cells, whereas *KCNQ4* was not detectable.

KCNQ2 was expressed in all utricle hair cells. Other classes of voltage-gated potassium channels were differentially expressed among hair cell subtypes. *KCNA10* and *KCNAB1* were exclusively detected in striolar type I hair cells, whereas *KCNA3* was specific to extrastriolar type II hair cells. *KCNA4* and *KCNH7* were found to be expressed in nascent hair cells that co-express *ATOH1*. Interestingly, expression of *KCNG4* only occurred in striolar type II hair cells.

Inwardly rectifying potassium channels, encoded by the *KCNJ* gene family, play an essential role in maintaining normal potassium homeostasis and the resting membrane potential (Meredith and Rennie, 2016). We detected *KCNJ2* expression in extrastriolar and striolar type II hair cells. *KCNJ5* and *KCNJ11* were specific to striolar type II hair cells, albeit at much lower levels than *KCNJ2*. Interestingly, we also found two *KCNJ* genes expressed in supporting cells. Whereas all supporting cells expressed *KCNJ16*, *KCNJ15* was only detected in striolar reversal zone-associated supporting cells. Two-pore domain (K2P) potassium channels, encoded by the *KCNK* gene family, generate background leak-type potassium currents. K2P channels are modulated by binding small ubiquitin-like modifiers (Plant et al., 2005). Chicken vestibular hair cells express *KCNK1* and *SUMO1* at high levels. Interestingly, *KCNK3* was specifically expressed in nascent hair cells that co-express ATOH1.

Nicotinic acetylcholine receptor subunits were detected in utricle hair cells. *CHRNA9* transcripts were present in all hair cells. *CHRNA10* was only found in striolar type I and type II hair cells and not in extrastriolar type II hair cells. In addition, *CHRNA1* was transiently expressed in nascent hair cells.

Supporting cells

In the chicken utricle, supporting cells are a permanent source for hair cells that are perpetually produced mitotically throughout the animal's life. Moreover, when hair cells die due to noise or other ototoxic damage, supporting cells serve as facultative stem cells to replace lost hair cells. Structurally, together with hair cells, they create a paracellular diffusion barrier at the apical surface of the sensory epithelium, the reticular lamina. Tight junctions provide structural integrity to the reticular lamina, and claudins are the principal components of tight junctions. We detected *CLDN1*, *CLDN8*, and *CLDN9*. Whereas *CLDN8* mRNA transcripts were higher in supporting cells than in hair cells, *CLDN1* and *CLDN9* expression were restricted to supporting cells. Tetraspanins are small membrane proteins that exhibit similar cell-cell adhesion capacities as claudins; some tetraspanins can directly bind to claudins (Harris et al., 2010). We identified multiple tetraspanins (*TSPAN5*, *TSPAN6*, *TSPAN13*, *TSPAN15*) in supporting cells and hair cells.

Supporting cells are connected through gap junctions that enable an exchange of small molecules and ions. Gap junctions consist of connexin proteins that form hemichannels between cells expressing connexin genes. We observed expression of connexin26 (*GJB2*) and connexin 30 (*GJB6*) in mature chicken vestibular supporting cells, and expectedly, hair cells did not express gap junction genes (Heller et al., 1998).

Transitional cells

The basic-helix-loop-helix transcription factor ATOH1 is essential for the differentiation of hair cells (Bermingham et al., 1999). Because hair cells turn over in the avian utricle and are continuously produced throughout life, we expected to detect *ATOH1* expression in the mature chicken utricle. We found that *ATOH1* was significantly enriched in the nascent hair cell group S6. This group also expresses the Notch ligands *DLL1*, *DLK2*, and *JAG2*, class III β-tubulins such as *TUBB3*, and the transcription factor *PROX1*. These genes have been all described as makers for nascent hair cells expressed early during hair cell differentiation (Adam et al., 1998; Cai et al., 2015; Lanford et al., 1999; Molea et al., 1999; Morrison et al., 1999; Stone et al., 2004). Along our proposed transitional cell trajectory, we found that high *HES5* expression in supporting cells is displaced by *HES1* in transitional supporting cells, followed by absent or low levels of HES genes in the *ATOH1*-expressing nascent hair cell group S6 (Table S1D). This sequence agrees with the previously proposed regulation of *ATOH1* through NOTCH signaling but also suggests more refined roles for individual effectors such as different HES and HEY genes, as well as potential crosstalk with other signaling pathways.

NHLH1 is another basic-helix-loop-helix gene that was discernible in the nascent hair cell group S6. *NHLH1* expression in mice is robust in young hair cells, becomes downregulated during hair cell maturation, and is no longer detected in adult inner ear tissue (Kruger et al., 2006; Scheffer et al., 2015). Cell type-defining gene expression examples such as *ATOH1* and *NHLH1* elevate the reconstructed trajectory to a resource for exploring genes that are expressed before, with, or after *ATOH1*. Tables S2 and S3 provide a resource for identifying such genes that could play important roles in the early differentiation process of hair cells.

Both trajectory branches of newly generated utricle hair cells arose from nascent group S6. This suggests that extrastriolar and striolar hair cells are generated from a common group of ATOH1-expressing cells. Parallel emergence of extrastriolar type II hair cells and striolar hair cells that further bifurcate into type I and striolar type II hair cells suggests that hair cell subtypes in the mature chicken utricle emerge directly from progenitor cells. This principal process has also been described in the developing chicken utricle (Ellwanger et al., 2018; Zhu et al., 2019). In contrast, in mice, studies suggest that type I hair cells develop first a type II-like hair cell phenotype or even thatthere is a transformation of fully differentiated type II hair cells into type I hair cells (Kirkegaard and Jorgensen, 2000; Masetto and Correia, 1997; Weisleder et al., 1995). Recent studies have demonstrated that in the neonatal mouse utricle, new hair cells develop into type II hair cells and that emerging type I hair cells downregulate SOX2 when they acquire a calyx (McInturff et al., 2018; Warchol et al., 2019). Our findings suggest that vestibular hair cell subtype specification might differ between animal classes.

Our trajectory reconstruction positioned cell group S3 between the ATOH1-expressing nascent hair cell group and the supporting cells. We conclude that S3 represents a transitional supporting cell state that downregulates pan-supporting cell genes. GO analysis linked S3 to terms indicative of a transition into the mitotic cell cycle, whereas the dominant gene groups in the nascent hair cell group S6 were associated with hair cell differentiation. Postmitotic supporting cells of the adult mouse utricle can enter the cell cycle after c-myc

(*Myc*) overexpression (Burns et al., 2012b). *MYC* transcripts were highly enriched in the supporting cell group S3. We conclude that S3 cells represent supporting cells that transition out of quiescence toward mitosis and that S6 represents the subsequent hair cell fate (Figure 6).

In summary, we anticipate that our study will be a valuable resource for inner ear developmental biology, electrophysiology, and regenerative medicine. Our dataset offers a reference for transcriptomic comparisons of avian and mammalian inner ear cells in the context of hair cell loss or other pathologies. In sharp contrast to mammals, the vestibular sensory epithelia of birds functionally recover from hair cell loss. Knowledge of the baseline and homeostatic gene expression dynamics of the undamaged avian utricle is the basis for future studies of hair cell regeneration. This, in turn, is crucial for identifying missing signals in mammals that could be promising candidates for activating mammalian hair cell regeneration to treat balance disorders and hearing loss.

Limitations of the study

The anatomic simplicity of the avian utricle allowed us to identify the major hair cell subtypes as well as subtle differences in gene expression among supporting cells. High sequencing depth limited our study to a few hundred cells, which could account for potentially missing rare cell states or the unresolved trajectory from postmitotic progenitor cells back to supporting cells. Consequently, the path of postmitotic transition of daughter cells back to supporting cells is latent and not evident in the reconstructed trajectory. Alternatively, after mitosis, cells that do not differentiate into new hair cells might reverse back into supporting cells by upregulating the same genes that are downregulated during dedifferentiation, and the resulting transition is simply the reversal of the S3 trajectory. Future comparative studies aimed to discriminate between natural turnover production of hair cells and hair cell regeneration might require larger sample sizes.

STAR★METHODS

RESOURCE AVAILABILITY

Lead contact—Further information and requests for reagents may be directed to the lead contact, Stefan Heller (hellers@stanford.edu).

Materials availability—The study did not generate new unique reagents.

Data and code availability

- The RNA sequencing data generated in this paper is stored in a CSV table and a SingleCellExperiment container that are publicly available at Mendeley Data. The DOI is listed in the key resources table.
- The RNA sequencing data has been deposited at Gene Expression Omnibus. The accession number is listed in the key resources table.

- The data is also available at gEAR, a gene Expression Analysis Resource (https://umgear.org/) (Orvis et al. 2021), *via* PERMA-LINK https://umgear.org/p?l=GgUtricleP7.
- No original code was developed.
- Any additional information required to reanalyze the data reported in this paper is available from the lead contact upon request.

EXPERIMENTAL MODEL AND SUBJECT DETAILS

Dissection of the chicken utricle—Fertilized chicken eggs were purchased from AA Laboratory Eggs Inc., Westminster, CA. The eggs were maintained at 39°C in a humidified incubator and, after 19 days of development, moved into a separate incubator for hatching. The hatchlings were transferred to a brooder cage equipped with an infrared heat lamp, chick starter feed, and water. All animal procedures were approved by the Stanford University Institutional Animal Care and Use Committee.

P7 chickens of both sexes were euthanized with CO_2 inhalation, the heads were bisected, the brain was removed, and the temporal bones were excised with surgical scissors, then placed into ice-cold Medium 199. Utricles were dissected and processed for single-cell RNA-sequencing, immunocytochemistry, or *in situ* mRNA detection.

METHOD DETAILS

Single-cell Isolation, flow Cytometry and RNA-Sequencing—Utricles were dissected in ice-cold Medium 199, otolithic membranes were mechanically removed, and tissue was incubated in thermolysin (0.5 mg/mL M199 medium) for 20 min at 37°C. Thermolysin activity was attenuated with 10% FBS in M199. The sensory epithelia were carefully peeled off from the underlying stromal cells using a 30-gauge ½-inch hypodermic needle attached to a 1 mL syringe. For each experiment, we pooled 4–8 sensory epithelia. The epithelia were dissociated using 1X Accutase for 20 min at 37°C, followed by mild mechanical trituration, and washed twice with PBS using a centrifugation step (300 x g, 5 min, room temperature (RT)).

Viable single cells were isolated with a Becton Dickinson FACSAria Fusion flow cytometer (Ellwanger et al., 2018). Two independent batches of 270 cells were deposited into individual wells of 96-well plates, prefilled with 4 μL of a premade lysis solution with 1 U/μl of recombinant RNase inhibitor, 0.1% Triton X-100, 2.5 mM dNTP mix, 2.5 μM oligo d(T)30 VN (5'-AAGCAGTGGTATCAACGCAGAGTACT30VN-3', IDT). Plates containing sorted cells were immediately sealed, frozen on dry ice, and stored at −80°C.

Single-cell RNA-seq was performed via Picelli and colleagues' method (Picelli et al., 2014) using SMARTscribe for reverse transcription followed by 22 amplification cycles. Amplified cDNAs were purified by AMPure Beads cleanup using a Biomek FX automated platform and assessed with a fragment analyzer (Agilent) for quantitation and quality assurance. Barcoded libraries were synthesized using a scaled-down Nextera XT protocol (Mora-Castilla et al., 2016) in a total volume of 4 μL. A total of 384 libraries were pooled and paired-end sequenced (2 × 150 bp) on a NextSeq 500/550 High Output flow cell. Raw

reads in FASTQ format were aligned to the NCBI *Gallus gallus* v6.0 (GCF_000002315.6) reference genome using custom scripts on the Sherlock Supercomputer Cluster (Stanford). The FastQC tool was used to run an initial quality control check on the raw sequence data. Sequencing reads were mapped by STAR aligner, and the transcriptome BAM files were quantified by RSEM.

Scater was used to perform the quality control of the raw count expression matrix of 379 cells and 17,557 genes. ERCC spike-in transcripts, 57 information-poor cells, and 3,914 low-level expressed genes were removed from the count matrix before read count normalization using SCnorm (Bacher et al., 2017). The CellTrails R package was then utilized for cluster and trajectory analyses (Ellwanger et al., 2018; Zhu et al., 2019).

EdU Injections—5-Ethynyl-2′-deoxyuridine (EdU, 100 mg/kg in PBS) was administered subcutaneously in P6 chickens. Utricles were dissected 24 h after EdU administration. EdU incorporation into DNA in utricular vibratome sections was detected using the Click-iT EdU Alexa Fluor 647 Imaging Kit (Thermo Fisher Scientific, C10340) before proceeding to immunocytochemistry or hybridization chain reaction.

Vibratome sectioning—The temporal bones from P7 chickens were placed into 4% paraformaldehyde in RNase-free PBS and fixed overnight at 4°C. Utricles were dissected and incubated in 0.25 M EDTA in PBS overnight at 4°C until the otoconia appeared clear. EDTA treatment was omitted for *in situ* mRN*A* detection. The fixed tissues were equilibrated for 5 min in RNase-free PBS at 55°C, followed by two 15 min incubations, first in 2%, and then in 4% low gelling temperature agarose in RNase-free PBS at 55°C. Utricles were transferred into disposable molds and embedded in bubble-free 4% low gelling temperature agarose. Utricles were sectioned transversely anterior-to posterior in cold RNase-Free PBS using a Leica VT1200 vibratome (80 μm thickness, 1 mm amplitude, 0.8 mm/s speed). Sections were decanted onto a black Sylgard® 184 silicone plate (Montgomery and Cox, 2016). Round agarose cylinders with individual sections were obtained with a 1.5 mm biopsy punch. For immunohistochemistry, sections were transferred into cold PBS. For *in situ* mRNA detection, sections were washed with 50% methanol in RNase-Free PBS for 5 min, then stored in 100% methanol at −20°C.

Immunocytochemistry of vibratome sections and whole utricles—Vibratome sections were permeabilized for 30 min with 1% Triton X-100 in PBS at RT, then blocked for 3–4 h at RT with a PBS-based blocking solution containing 1% BSA, 5% donkey serum, and 0.1% Triton X-100. Sections were incubated at 4°C overnight in blocking solution with diluted primary antibodies. The next day, sections were washed three times for 15 min in 0.2% Triton X-100 in PBS and incubated for 1–2 h in blocking solution with diluted secondary antibodies at RT. After washing three times for 15 min with 0.2% Triton X-100 in PBS, sections were exposed for 15 min to 4,6-Diamidino-2-phenylindole (DAPI) to visualize nuclei, and phalloidin to visualize F-ACTIN. Finally, sections were rinsed three times for 15 min with 0.2% Triton X-100 in PBS and three times for 15 min with PBS. The sections were mounted in FluorSave™ Reagent using a Secure-Seal™ Spacer attached to a glass slide. Coverslips were sealed with nail polish.

Fixed and decalcified whole utricles were rinsed three times with PBS for 15 min, permeabilized for 30 min with 1% Triton X-100 in PBS and blocked for 3–4 h at RT with blocking solution. Utricles were then incubated at 4°C overnight in blocking solution with primary antibodies. Tissues were washed three times for 15 min with 0.2% Triton X-100 in PBS and incubated for 1–2 h at RT in blocking solution with secondary antibodies. DAPI was used to visualize nuclei. Finally, utricles were washed three times for 15 min with 0.2% Triton X-100 in PBS and three times for 15 min with PBS.

In situ* hybridization and hybridization chain reaction (HCR)—In situ* hybridization and HCR were carried out using the Secure-Seal™ hybridization sealing system attached to a Gold Seal™ UltraStick™ Adhesion Microscope Slide. 6–8 vibratome sections with a thickness between 40 and 50 μm in methanol were fixed onto a Gold Seal UltraStick Adhesion Microscope Slide by allowing the methanol to evaporate. The hybridization chamber was firmly attached to the slide with the vibratome sections aligned with its center. *In situ* hybridization and HCR were generally performed as described (Benkafadar et al., 2021; Harland, 1991; Janesick et al., 2021).

RNA probe synthesis templates of ~500 bp were created via PCR amplification from whole inner ear cDNA with oligonucleotide primer pairs featuring a T7 promoter sequence in the 3′ end of the reverse primer. Primer sequences are listed in Table S4. Probes were transcribed using the MEGAscript® T7 kit and digoxigenin-11-UTP ribonucleoside triphosphate mix.

Vibratome sections were rehydrated in 50% methanol, 50% 0.1% Tween 20 in RNase-free PBS for 5 min, washed once in 0.1% Tween 20 in RNase-free PBS and permeabilized with 10 μg/mL Proteinase K for 8 min at RT. Hybridization with digoxigenin-labeled probes (0.5 ng/μL) was conducted overnight at 55–60°C. Secure-Seal hybridization sealing system was sealed with 3M VHB Adhesive Seal Tabs. The next day, sections were washed with 2X SSC for 20 min at 55°C, exposed to 2X SSC and 1:1000 RNase Cocktail for 30 min at 37°C, and then washed in 0.2X SSC for 20 min at 55°C. Digoxigenin-labeled RNA was visualized with diluted Anti-Digoxigenin-AP followed by BM-Purple detection and 10 min fixation in 4% paraformaldehyde. Sections were mounted in 80% glycerol in PBS with a Secure-Seal™ Spacer, and imaged with a Leica DM2000 microscope, HCX Plan-Apochromat 40x/1.30 objective, oil immersion, using a Nikon D7000 color camera, 1.6X projection lens/adapter and digiCamControl software (V2.1.1.0). Images were manually tiled and merged using Microsoft Image Composite Editor (V2.0.3.0).

HCR was conducted as previously described (Benkafadar et al., 2021; Choi et al., 2018; Janesick et al., 2021). DAPI was added in PBS prior to mounting with a Secure-Seal Spacer in CitiFluor CFM3 media.

Vibratome sections and whole utricles were mounted in FluorSave Reagent using a Secure-Seal™ Spacer attached to a glass slide. The coverslips were sealed with clear nail polish. Imaging was conducted with Plan-Apochromat 20x/0.8 M27 and Plan-Apochromat 40x/1.3 NA oil DIC UV-IRM27 objectives. Digital zoom was adjusted between 0.6 and 0.9. Confocal z-stacks were collected with 6% overlap, tiling set to bounding grid mode, using

a Zeiss LSM 880 Airyscan laser scanning confocal microscope, and processed with Zen software.

QUANTIFICATION AND STATISTICAL ANALYSIS

For single-cell RNA-seq data analysis, we used the following R packages: scater, SCnorm, CellTrails, and SingleCellExperiment. For ranking differential gene expression, we utilized the Mann-Whitney U test, also known as the Wilcoxon rank-sum test in R (wilcox.test). Additional details on statistical analysis are provided in the figure legends. Pathway enrichment analysis was performed using g:Profiler and Cytoscape (Raudvere et al., 2019; Shannon et al., 2003). Differential expression dynamics for the trajectories were assessed by testing the significance of the smooth term (i.e., the pseudo-temporal location) of the generalized additive model fitted by CellTrails using the R package gam.

Supplementary Material

Refer to Web version on PubMed Central for supplementary material.

ACKNOWLEDGMENTS

Single-cell processing and sequencing were conducted at the Stanford Functional Genomics Facility, and we thank M.C. Yee and S. Sim for their assistance. Imaging was done in the OHNS microscopy core facility, and we thank Dr. P. Atkinson, and M. Bartho for their support. We thank Y. Song and R. Hertzano for cooperation with gEAR (funded by NIH grant DC019370) and the Heller laboratory for fruitful discussions and review of the manuscript. The Stanford Shared FACS Facility and the Stanford Functional Genomics Facility are supported by NIH grants S10OD018220 and 1S10OD021763. Funding was provided by School of Medicine Dean's Post-doctoral Fellowship (A.J., N.B.) and the A.P. Giannini Foundation (A.J.), the Hearing Restoration Project consortium of the Hearing Health Foundation, the Stanford Initiative to Cure Hearing Loss, and NIH DC019619 (S.H.) and DC019683 (T.A.J.).

REFERENCES

Adam J, Myat A, Le Roux I, Eddison M, Henrique D, Ish-Horowicz D, and Lewis J (1998). Cell fate choices and the expression of Notch, Delta and Serrate homologues in the chick inner ear: parallels with Drosophila sense-organ development. Development 125, 4645–4654. [PubMed: 9806914]

Bacher R, Chu LF, Leng N, Gasch AP, Thomson JA, Stewart RM, Newton M, and Kendziorski C (2017). SCnorm: robust normalization of single-cell RNA-seq data. Nat. Methods 14, 584–586. [PubMed: 28418000]

Benkafadar N, Janesick A, Scheibinger M, Ling AH, Jan TA, and Heller S (2021). Transcriptomic characterization of dying hair cells in the avian cochlea. Cell Rep 34, 108902. [PubMed: 33761357]

Bermingham NA (1999). Math1: an essential gene for the generation of inner ear hair cells. Science 284, 1837–1841. [PubMed: 10364557]

Bermingham NA, Hassan BA, Price SD, Vollrath MA, Ben-Arie N, Eatock RA, Bellen HJ, Lysakowski A, and Zoghbi HY (1999). Math1: an essential gene for the generation of inner ear hair cells. Science 284, 1837–1841. [PubMed: 10364557]

Beurg M, Michalski N, Safieddine S, Bouleau Y, Schneggenburger R, Chapman ER, Petit C, and Dulon D (2010). Control of exocytosis by synaptotagmins and otoferlin in auditory hair cells. J. Neurosci 30, 13281–13290. [PubMed: 20926654]

Burns JC, Kelly MC, Hoa M, Morell RJ, and Kelley MW (2015). Single-cell RNA-Seq resolves cellular complexity in sensory organs from the neonatal inner ear. Nat. Commun 6, 8557. [PubMed: 26469390]

Burns JC, On D, Baker W, Collado MS, and Corwin JT (2012a). Over half the hair cells in the mouse utricle first appear after birth, with significant numbers originating from early postnatal

mitotic production in peripheral and striolar growth zones. Journal of the Association for Research in Otolaryngology : JARO 13, 609–627. [PubMed: 22752453]

Burns JC, Yoo JJ, Atala A, and Jackson JD (2012b). MYC gene delivery to adult mouse utricles stimulates proliferation of postmitotic supporting cells in vitro. PLoS One 7, e48704. [PubMed: 23119091]

Cai T, Jen HI, Kang H, Klisch TJ, Zoghbi HY, and Groves AK (2015). Characterization of the transcriptome of nascent hair cells and identification of direct targets of the Atoh1 transcription factor. J. Neurosci 35, 5870–5883. [PubMed: 25855195]

Chessum L, Matern MS, Kelly MC, Johnson SL, Ogawa Y, Milon B, McMurray M, Driver EC, Parker A, Song Y, et al. (2018). Helios is a key transcriptional regulator of outer hair cell maturation. Nature 563, 696–700. [PubMed: 30464345]

Choi HMT, Schwarzkopf M, Fornace ME, Acharya A, Artavanis G, Stegmaier J, Cunha A, and Pierce NA (2018). Third-generation in situ hybridization chain reaction: multiplexed, quantitative, sensitive, versatile, robust. Development 145.

Eatock RA (2018). Specializations for fast signaling in the amniote vestibular inner ear. Integr. Comp. Biol 58, 341–350. [PubMed: 29920589]

Ellwanger DC, Scheibinger M, Dumont RA, Barr-Gillespie PG, and Heller S (2018). Transcriptional dynamics of hair-bundle Morphogenesis revealed with CellTrails. Cell Rep 23, 2901–2914.e3. [PubMed: 29874578]

Fukuda M (2003). Molecular cloning, expression, and characterization of a novel class of synaptotagmin (Syt XIV) conserved from Drosophila to humans. J. Biochem 133, 641–649. [PubMed: 12801916]

Garcia-Anoveros J, Clancy JC, Foo CZ, Garcia-Gomez I, Zhou Y, Homma K, Cheatham MA, and Duggan A (2022). Tbx2 is a master regulator of inner versus outer hair cell differentiation. Nature 605, 298–303. [PubMed: 35508658]

Giese APJ, Tang YQ, Sinha GP, Bowl MR, Goldring AC, Parker A, Freeman MJ, Brown SDM, Riazuddin S, Fettiplace R, et al. (2017). CIB2 interacts with TMC1 and TMC2 and is essential for mechanotransduction in auditory hair cells. Nat. Commun 8, 43. [PubMed: 28663585]

Goodyear RJ, Gates R, Lukashkin AN, and Richardson GP (1999). Hair-cell numbers continue to increase in the utricular macula of the early posthatch chick. J. Neurocytol 28, 851–861. [PubMed: 10900089]

Goodyear RJ, Legan PK, Christiansen JR, Xia B, Korchagina J, Gale JE, Warchol ME, Corwin JT, and Richardson GP (2010). Identification of the hair cell soma-1 antigen, HCS-1, as otoferlin. Journal of the Association for Research in Otolaryngology : JARO 11, 573–586. [PubMed: 20809368]

Harland RM (1991). In situ hybridization: an improved whole-mount method for Xenopus embryos. Methods Cell Biol 36, 685–695. [PubMed: 1811161]

Harris HJ, Davis C, Mullins JG, Hu K, Goodall M, Farquhar MJ, Mee CJ, McCaffrey K, Young S, Drummer H, et al. (2010). Claudin association with CD81 defines hepatitis C virus entry. J. Biol. Chem 285, 21092–21102. [PubMed: 20375010]

Hawkins RD, Helms CA, Winston JB, Warchol ME, and Lovett M (2006). Applying genomics to the avian inner ear: development of subtractive cDNA resources for exploring sensory function and hair cell regeneration. Genomics 87, 801–808. [PubMed: 16516437]

Heller S, Sheane CA, Javed Z, and Hudspeth AJ (1998). Molecular markers for cell types of the inner ear and candidate genes for hearing disorders. Prod. of the Natl. Acad. Sci. USA 95, 11400–11405.

Janesick A, Scheibinger M, Benkafadar N, Kirti S, Ellwanger DC, and Heller S (2021). Cell-type identity of the avian cochlea. Cell Rep 34, 108900. [PubMed: 33761346]

Janesick AS, and Heller S (2019). Stem cells and the bird cochlea-where is everybody? Cold Spring Harb Perspect Med 9.

Jorgensen JM (1989). Number and distribution of hair cells in the utricular macula of some avian species. J. Morphol 201, 187–204. [PubMed: 29865667]

Kirkegaard M, and Jorgensen JM (2000). Continuous hair cell turnover in the inner ear vestibular organs of a mammal, the Daubenton's bat (Myotis daubentonii). Naturwissenschaften 87, 83–86. [PubMed: 10663140]

Kruger M, Schmid T, Kruger S, Bober E, and Braun T (2006). Functional redundancy of NSCL-1 and NeuroD during development of the petrosal and vestibulocochlear ganglia. Eur. J. Neurosci 24, 1581–1590. [PubMed: 17004922]

Lanford PJ, Lan Y, Jiang R, Lindsell C, Weinmaster G, Gridley T, and Kelley MW (1999). Notch signalling pathway mediates hair cell development in mammalian cochlea. Nat. Genet 21, 289–292. [PubMed: 10080181]

Martin KC, and Ephrussi A (2009). mRNA localization: gene expression in the spatial dimension. Cell 136, 719–730. [PubMed: 19239891]

Masetto S, and Correia MJ (1997). Electrophysiological properties of vestibular sensory and supporting cells in the labyrinth slice before and during regeneration. J. Neurophysiol 78, 1913–1927. [PubMed: 9325360]

McInturff S, Burns JC, and Kelley MW (2018). Characterization of spatial and temporal development of Type I and Type II hair cells in the mouse utricle using new cell-type-specific markers. Biol Open 7.

Meredith FL, and Rennie KJ (2016). Channeling your inner ear potassium: K(+) channels in vestibular hair cells. Hear. Res 338, 40–51. [PubMed: 26836968]

Molea D, Stone JS, and Rubel EW (1999). Class III beta-tubulin expression in sensory and nonsensory regions of the developing avian inner ear. J. Comp. Neurol 406, 183–198. [PubMed: 10096605]

Montgomery SC, and Cox BC (2016). Whole mount dissection and Immunofluorescence of the adult mouse cochlea. J Vis Exp

Mora-Castilla S, To C, Vaezeslami S, Morey R, Srinivasan S, Dumdie JN, Cook-Andersen H, Jenkins J, and Laurent LC (2016). Miniaturization Technologies for Efficient single-cell library preparation for next-generation sequencing. J. Lab. Autom 21, 557–567. [PubMed: 26891732]

Morrison A, Hodgetts C, Gossler A, Hrabe de Angelis M, and Lewis J (1999). Expression of Delta1 and Serrate1 (Jagged1) in the mouse inner ear. Mech. Dev 84, 169–172. [PubMed: 10473135]

Orvis J, Gottfried B, Kancherla J, Adkins RS, Song Y, Dror AA, Olley D, Rose K, Chrysostomou E, Kelly MC, et al. (2021). gEAR: Gene Expression Analysis Resource portal for community-driven, multi-omic data exploration. Nat. Methods 18, 843–844. 10.1038/s41592-021-01200-9. [PubMed: 34172972]

Picelli S, Faridani OR, Bjorklund AK, Winberg G, Sagasser S, and Sandberg R (2014). Full-length RNA-seq from single cells using Smart-seq2. Nat. Protoc 9, 171–181. [PubMed: 24385147]

Plant LD, Rajan S, and Goldstein SA (2005). K2P channels and their protein partners. Curr. Opin. Neurobiol 15, 326–333. [PubMed: 15922586]

Ranum PT, Goodwin AT, Yoshimura H, Kolbe DL, Walls WD, Koh JY, He DZZ, and Smith RJH (2019). Insights into the biology of hearing and deafness revealed by single-cell RNA sequencing. Cell Rep 26, 3160–3171.e3. [PubMed: 30865901]

Raudvere U, Kolberg L, Kuzmin I, Arak T, Adler P, Peterson H, and Vilo J (2019). g:Profiler: a web server for functional enrichment analysis and conversions of gene lists (2019 update). Nucleic Acids Res 47, W191–W198. [PubMed: 31066453]

Safieddine S, and Wenthold RJ (1999). SNARE complex at the ribbon synapses of cochlear hair cells: analysis of synaptic vesicle- and synaptic membrane-associated proteins. Eur. J. Neurosci 11, 803–812. [PubMed: 10103074]

Scheffer DI, Shen J, Corey DP, and Chen ZY (2015). Gene expression by mouse inner ear hair cells during development. J. Neurosci 35, 6366–6380. [PubMed: 25904789]

Scheibinger M, Ellwanger DC, Corrales CE, Stone JS, and Heller S (2018). Aminoglycoside damage and hair cell regeneration in the chicken utricle. JARO 19, 17–29. [PubMed: 29134476]

Shannon P, Markiel A, Ozier O, Baliga NS, Wang JT, Ramage D, Amin N, Schwikowski B, and Ideker T (2003). Cytoscape: a software environment for integrated models of biomolecular interaction networks. Genome Res 13, 2498–2504. [PubMed: 14597658]

Stone JS, Shang JL, and Tomarev S (2004). cProx1 immunoreactivity distinguishes progenitor cells and predicts hair cell fate during avian hair cell regeneration. Dev Dyn 230, 597–614. [PubMed: 15254895]

Strenzke N, Chanda S, Kopp-Scheinpflug C, Khimich D, Reim K, Bulankina AV, Neef A, Wolf F, Brose N, Xu-Friedman MA, et al. (2009). Complexin-I is required for high-fidelity transmission at the endbulb of Held auditory synapse. J. Neurosci 29, 7991–8004. [PubMed: 19553439]

Uthaiah RC, and Hudspeth AJ (2010). Molecular anatomy of the hair cell's ribbon synapse. J. Neurosci 30, 12387–12399. [PubMed: 20844134]

Wagner EF, and Nebreda AR (2009). Signal integration by JNK and p38 MAPK pathways in cancer development. Nat. Rev. Cancer 9, 537–549. [PubMed: 19629069]

Warchol ME, Massoodnia R, Pujol R, Cox BC, and Stone JS (2019). Development of hair cell phenotype and calyx nerve terminals in the neonatal mouse utricle. J. Comp. Neurol 527, 1913–1928. [PubMed: 30724338]

Warchol ME, and Montcouquiol M (2010). Maintained expression of the planar cell polarity molecule Vangl2 and reformation of hair cell orientation in the regenerating inner ear. JARO 11, 395–406. [PubMed: 20177731]

Warchol ME, and Speck JD (2007). Expression of GATA3 and tenascin in the avian vestibular maculae: normative patterns and changes during sensory regeneration. J. Comp. Neurol 500, 646–657. [PubMed: 17154269]

Weisleder P, Tsue TT, and Rubel EW (1995). Hair cell replacement in avian vestibular epithelium: supporting cell to type I hair cell. Hear. Res 82, 125–133. [PubMed: 7744708]

Wersall J (1956). Studies on the structure and innervation of the sensory epithelium of the cristae ampulares in the Guinea pig; a light and electron microscopic investigation. Acta Otolaryngol Suppl 126, 1–85. [PubMed: 13326368]

Wiwatpanit T, Lorenzen SM, Cantu JA, Foo CZ, Hogan AK, Marquez F, Clancy JC, Schipma MJ, Cheatham MA, Duggan A, et al. (2018). Trans-differentiation of outer hair cells into inner hair cells in the absence of INSM1. Nature 563, 691–695. [PubMed: 30305733]

Zhu Y, Scheibinger M, Ellwanger DC, Krey JF, Choi D, Kelly RT, Heller S, and Barr-Gillespie PG (2019). Single-cell proteomics reveals changes in expression during hair-cell development. Elife 8.

Highlights

- Markers for spatially distinct hair cell and supporting cell groups
- Trajectories of gene expression dynamics during hair cell turnover
- Candidate genes that are active during hair cell generation
- Resource of cell-type-specific gene expression in the mature avian utricle

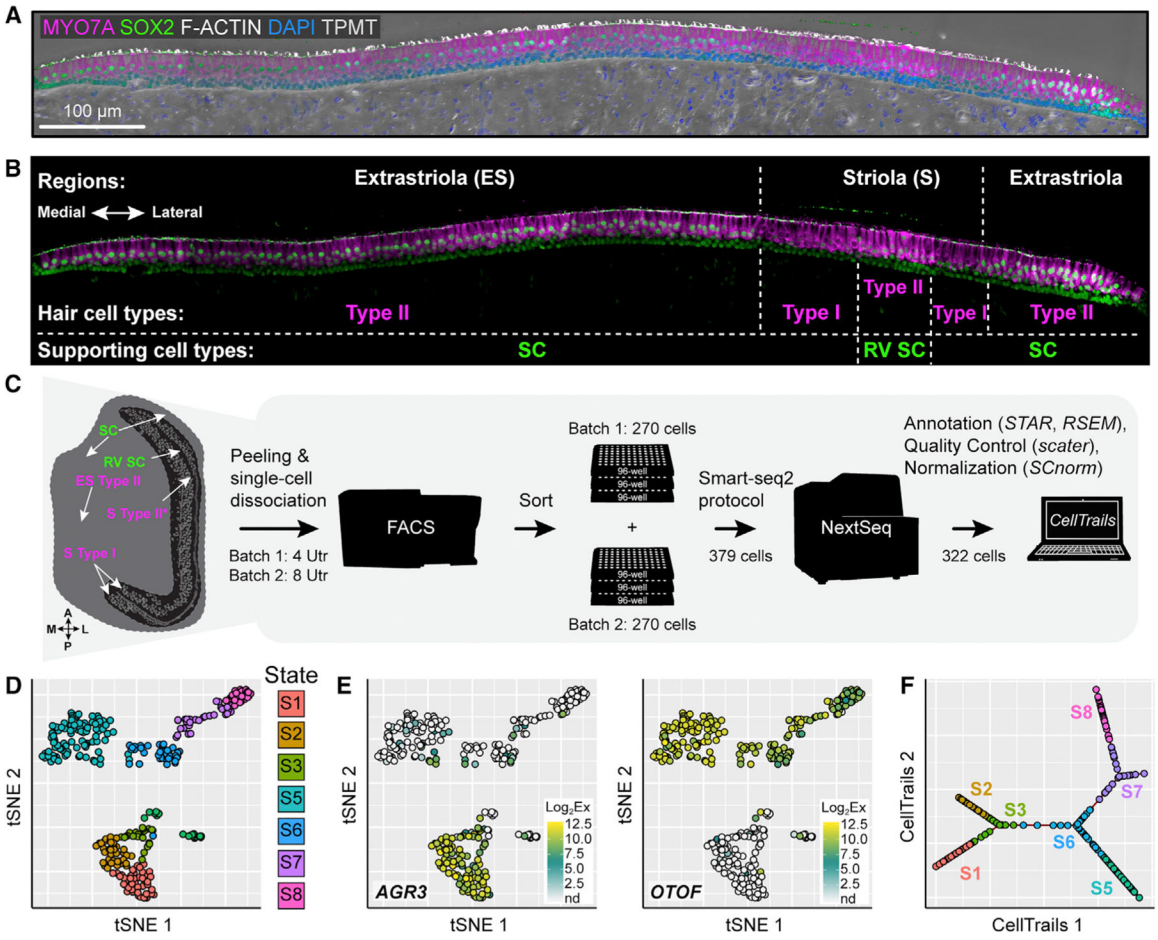

Figure 1. Identification of major cell groups

(A) Vibratome section of a P7 chicken utricle immunolabeled with antibodies to MYO7A (magenta) and SOX2 (green). F-ACTIN is visualized with phalloidin (white). Nuclei are labeled with DAPI (blue). The fluorescent image channels are projected onto the transmitted light detector image (TPMT).

(B) MYO7A and SOX2 labels type II hair cells located in the extrastriolar and striolar regions. MYO7A-positive and SOX2-negative type I hair cells are located in the striola. Associated with the line of cell polarity reversal (reversal zone = RV) in the striola are MYO7A-positive and SOX2-positive type II hair cells. Supporting cells (SC) express SOX2. Scale bar, 100 µm (for A and B).

(C) Two independent batches of sensory epithelia were peeled from the underlying stromal tissue and dissociated into single cells. Viable individual cells were flow cytometrically collected into single wells of 96-well plates. Each individual cell's mRNA was reverse transcribed, barcoded, amplified, quality controlled, quantified, and normalized. Libraries were generated and sequenced, annotated, and subjected to computational quality control. The final single-cell count matrix was normalized. Cell numbers for the individual steps are indicated.

(D) CellTrails identified eight distinct cellular states. Shown are 322 dots representing single utricle cells projected into two-dimensional space using t-distributed stochastic neighbor embedding (tSNE). Cells are colored by state affiliation, as indicated.
(E) Projection of *AGR3* and *OTOF* expression onto the tSNE plot. Log_2 expression scales for each gene are shown (Log_2Ex).
(F) Supporting cells (S1–S3) and hair cells (S5–S8) were ordered along a branching trajectory, displaying potential spatial and temporal relationships. See also Figure S1 and Table S1.

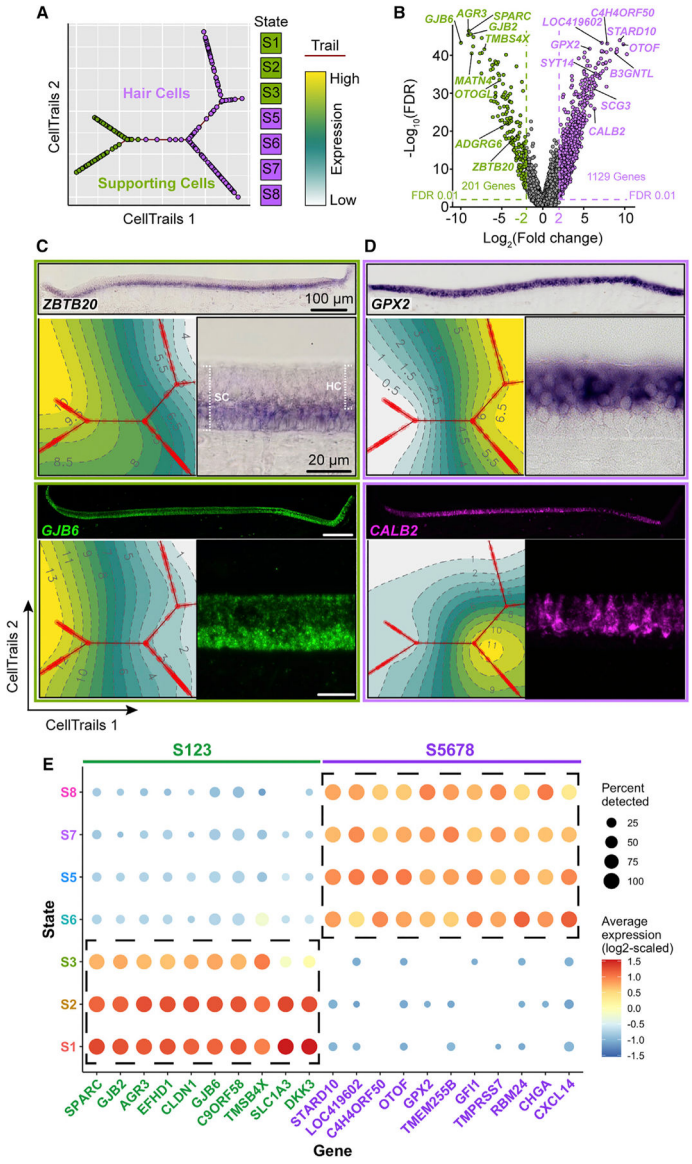

Figure 2. Supporting cells and hair cells

(A) CellTrails trajectory plot with supporting cell (green) and hair cell (magenta) groups.

(B) Volcano plot showing differential gene expression between supporting cells and hair cells. Colored dots represent genes with a $\log_2$-fold difference > 2 and a false discovery rate (FDR) < 0.01.

(C) *In situ* mRNA detection (DIG and HCR) images and CellTrails maps show expression of *ZBTB20* and *GJB6* in supporting cells.

(D) *In situ* mRNA detection and CellTrails maps of *GPX2* and *CALB2* show robust expression in hair cells. Scale bar, 20 µm (for C and D).

(E) DotPlot visualization of top 10 enriched genes in supporting cell (S123) and hair cell (S5678) groups. Dot size reflects percentage of cells in a state expressing each gene; dot color reflects expression level. See also Table S1.

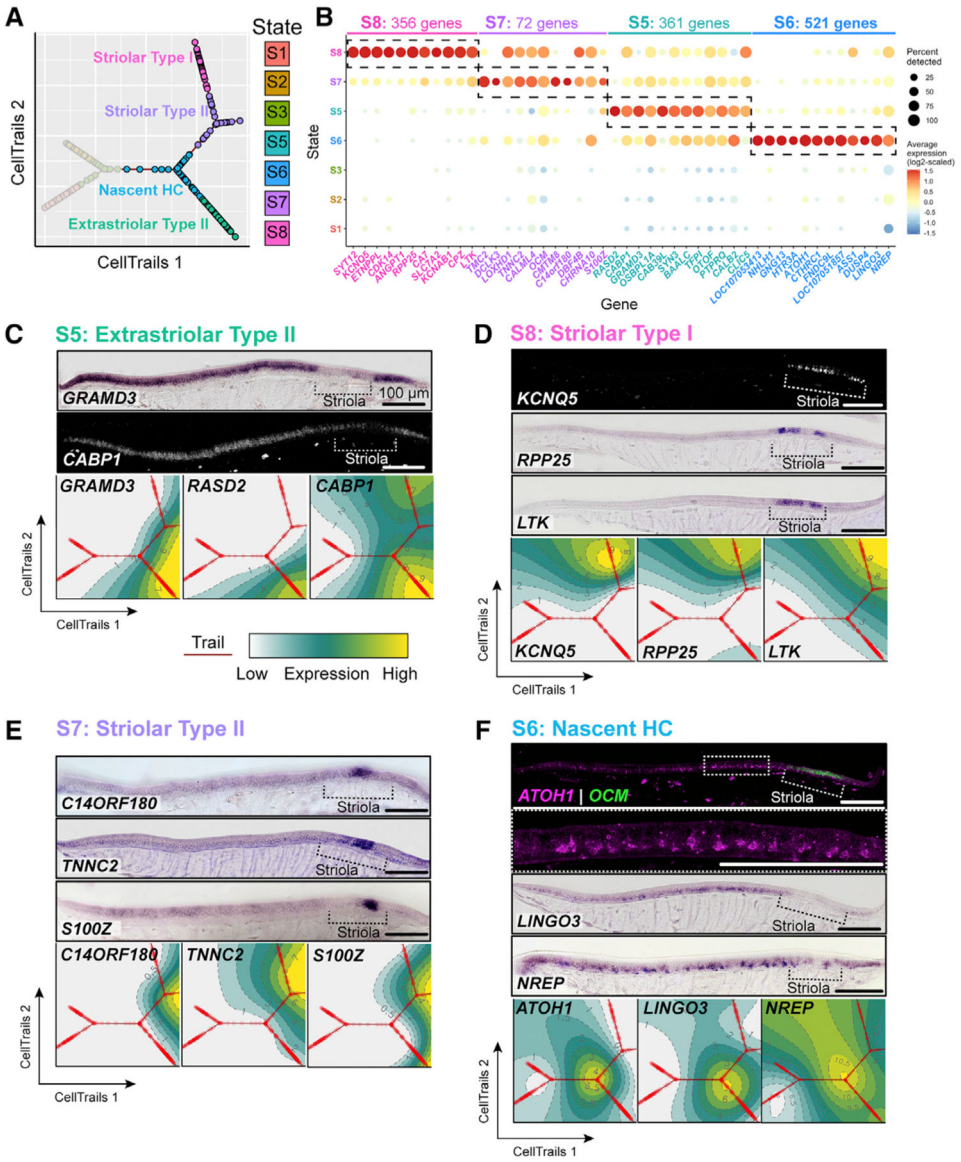

Figure 3. Distinct hair cell groups

(A) CellTrails trajectory plot with clusters S8 (striolar type I hair cells, magenta), S7 (striolar type II hair cells, purple), S5 (extrastriolar type II hair cells, green), and S6 (nascent hair cells, blue).

(B) DotPlot of top differentially enriched genes in hair cell groups (S5678). The numbers of genes per group have a $\log_2$-fold difference > 2 and a false discovery rate (FDR) < 0.01 (see Table S1).

(C) HCR and DIG *in situ* hybridization, as well as CellTrails maps for extrastriolar type II (S5) hair cell markers *GRAMD3*, *CABP1*, and *RASD2*.

(D) *In situ* mRNA detection and Celltrails Maps of *KCNQ5*, *RPP25*, and *LTK* mRNA in (S8) striolar type I hair cells.

(E) *In situ* mRNA detection and CellTrails maps for (S7) striolar type II hair cell markers *C14ORF180*, *TNNC2*, and *S100Z*.

(F) HCR and DIG *in situ* hybridization, as well as CellTrails maps for transitional hair cell markers *ATOH1*, *LINGO3*, and *NREP*. *OCM* mRNA is expressed by striolar hair cells. Scale bar, 100 μm (for C, D, E, and F). See also Figures S2–S4, and Table S1.

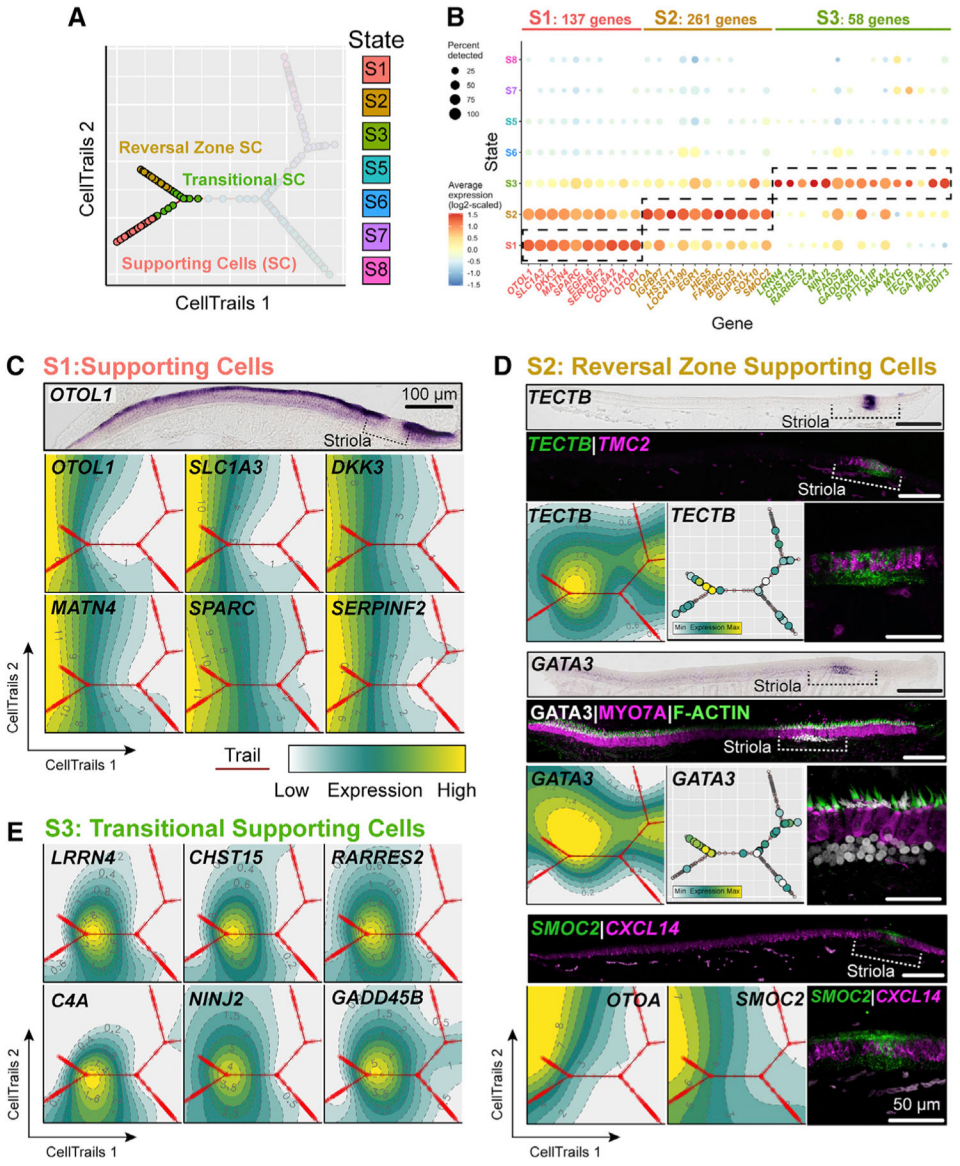

Figure 4. Distinct supporting cell groups

(A) CellTrails trajectory plot with supporting cell cluster S1, reversal zone supporting cells S2, and transitional supporting cells S3.

(B) DotPlot of top differentially enriched genes in supporting cell groups S1, S2, and S3. Differential expressed genes (DEG) analysis revealed 137 S1-, 261 S2-, and 58 S3-specific genes with a $\log_2$-fold difference > 2 and a false discovery rate (FDR) < 0.01 (see Table S1).

(C) *In situ* hybridization detection of *OTOL1* mRNA in supporting cells. The CellTrails maps show the projected higher gene expression levels for *OTOL1*, *SLC1A3*, *DKK3*, *MATN4*, *SPARC*, and *SERPINF2* in the S1 branch. Scale bar, 100 µm.

(D) *TECTB* mRNA is distinctively detectable in reversal zone striolar supporting cells (S2). *GATA3* mRNA and protein are associated with reversal zone striolar supporting cells along with *SMOC2* mRNA expression. *CXCL14* mRNA is detected in hair cells. Scale bar, 50 µm.

(E) CellTrails maps highlight the transient expression dynamics of *LRRN4*, *CHST15*, *RARRES2*, *C4A*, *NINJ2*, and *GADD45B* in transitional supporting cells S3. See also Figure S5 and Table S1.

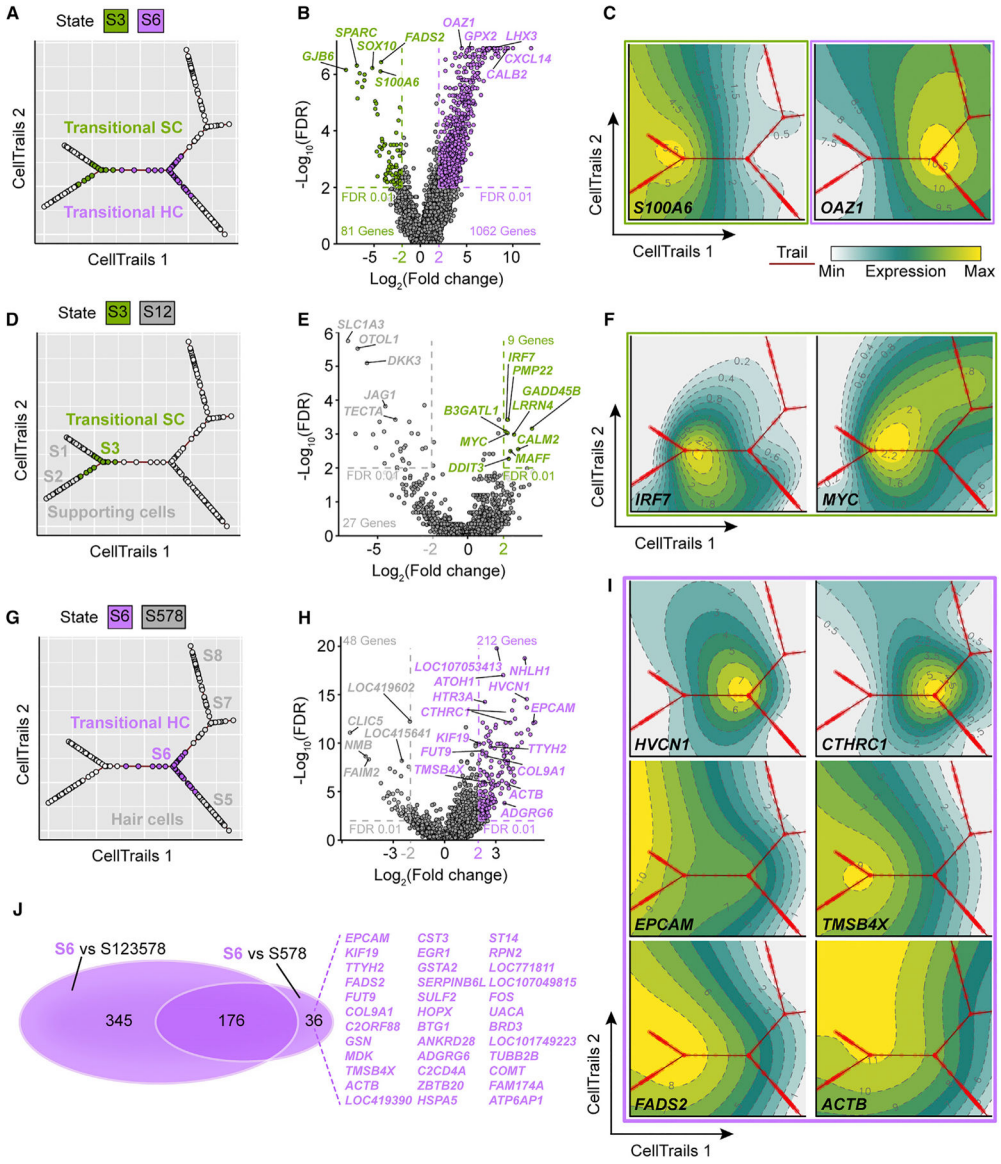

Figure 5. Transitional supporting cells and nascent hair cells

(A) CellTrails trajectory plot with clusters transitional supporting cells (S3) and emerging hair cells (S6) highlighted in green and magenta, respectively.

(B) Volcano plot showing differential gene expression between clusters S3 and S6.

(C) CellTrails maps for the differentially expressed S3 and S6 marker genes *S100A6* and *OAZ1*.

(D–F) CellTrails trajectory plot (D) and differential gene expression results (E) for cluster S3 (transitional supporting cells, green) in comparison with all other supporting cells (S1 and S2, gray). CellTrails maps (F) show that *IRF7* and *MYC* are distinctive markers for S3.

(G–I) CellTrails trajectory plot (G) and differential gene expression results (H) for cluster S6 (transitional hair cells, magenta) in comparison with all other hair cells (S5, S7, and S8, gray). CellTrails maps for S6 markers *HVCN1* and *CTHRC1*, as well as CellTrails maps

that illustrate declining supporting cell gene expression of *EPCAM*, *TMSB4X*, *FADS2*, and *ACTB* in cluster S6 cells.

(J) Venn diagram of gene expression comparisons and list of 36 genes that discriminate cluster S6 cells from mature hair cells. See also Table S1.

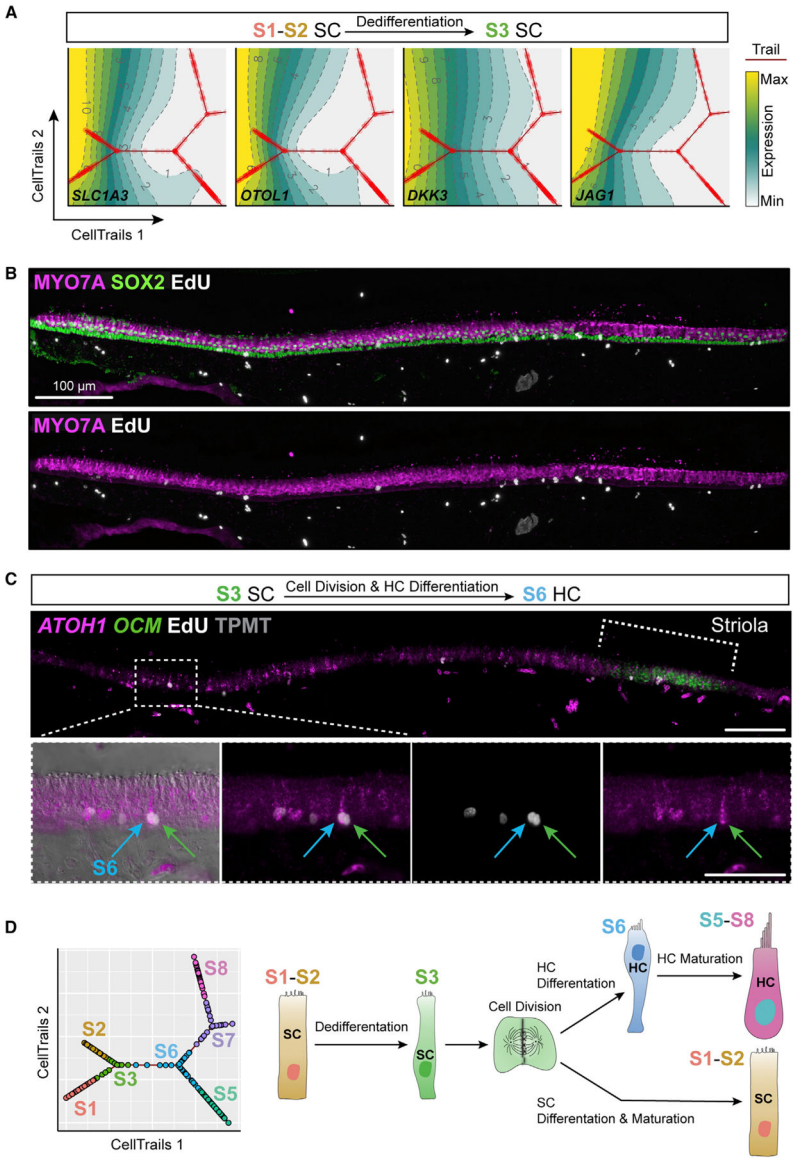

Figure 6. Natural hair cell generation in the P7 utricle

(A) Substantial downregulation of supporting cell markers *SLC1A3*, *OTOL1*, *DKK3*, and *JAG1* indicates a dedifferentiation of transitional S3 supporting cells.

(B) Vibratome section of a P7 chicken utricle immunolabeled with antibodies to MYO7A (magenta) and SOX2 (green). EdU was administrated 24 h before; pairs of EdU-labeled nuclei (white) were apparent throughout the sensory epithelium.

(C) Example of in-plane EdU-positive nuclei doublets. One nucleus is associated with an *ATOH1* mRNA expressing cell (S6, blue arrow), and the other EdU-positive cell (green arrow) is en route to becoming a supporting cell. Scale bar, 100 µm (for B and C); 40 µm for inset.

(D) Supporting cells in the chicken utricle (S1, S2) can dedifferentiate (S3), divide, and the resulting daughter cells differentiate into new hair cells (S6 → S5/7/8) and new supporting cells, which closes the cycle of hair cell turnover. See also Figure S7, Tables S2 and S3.

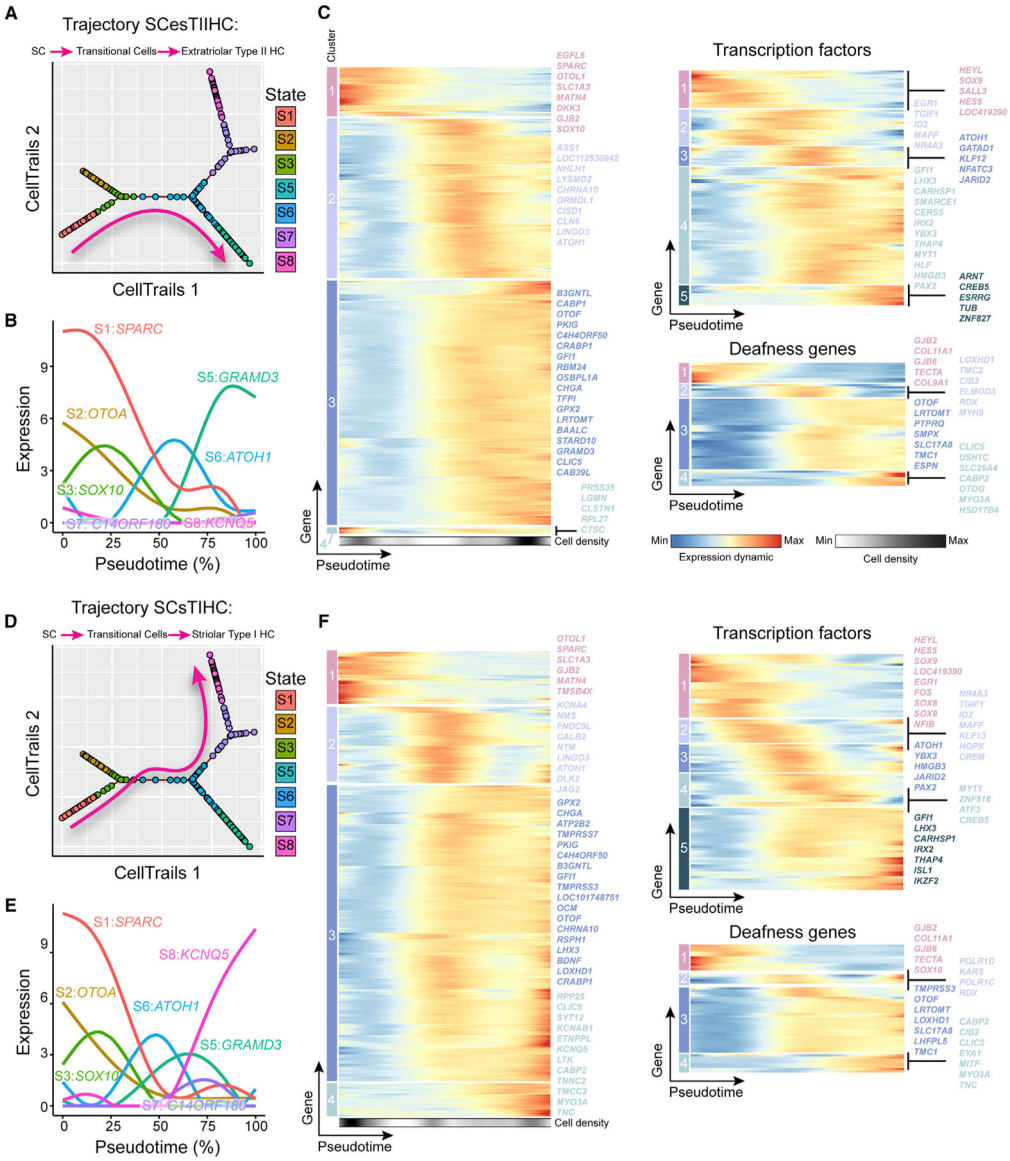

Figure 7. Gene expression dynamics toward extrastriolar type II and striolar type I hair cells

(A) CellTrails trajectory plot with the extrastriolar type II trajectory highlighted with a magenta arrow. The trajectory connects cells from supporting cells to extrastriolar hair cells, S1➔S3➔S6➔S5.

(B) Expression dynamics of $\log_2$ expression levels for state-specific marker genes along the extrastriolar trajectory.

(C) Heatmap visualization of gene expression dynamics for all genes, transcription factors, and deafness genes along the extrastriolar trajectory. Genes with similar dynamics are clustered.

(D) CellTrails trajectory plot with the striolar type I hair cell trajectory highlighted with a magenta arrow. The trajectory connects cells from supporting cells to type I hair cells, S1➔S3➔S6➔S7➔S8.

(E) Expression dynamics of $\log_2$ expression levels for state-specific marker genes along the striolar trajectory.

(F) Heatmap visualization of gene expression dynamics for all genes, transcription factors, and deafness genes along the striolar trajectory. Genes with similar dynamics are clustered. See also Figure S7 and Tables S2 and S3.

KEY RESOURCES TABLE

REAGENT or RESOURCE	SOURCE	IDENTIFIER
Antibodies		
Rabbit anti Myosin-7a (1:1000)	Proteus Biosciences	25-6790; RRID: AB_10015251
Mouse anti Myosin-7a (1:50)	DSHB	MYO7A 138-1; RRID: AB_2282417
Goat anti-Gata3 (1:200)	Thermo Fisher Scientific	AF2605; RRID: AB_2108571
Goat anti-Sox2 (1:100)	Santa Cruz Biotechnology	sc-17320; RRID: AB_2286684
Rabbit anti-Tectb (1:200)	Gifted by Dr. Guy Richardson, U of Sussex	N/A
Donkey anti-Rabbit IgG, Alexa Fluor 546 (1:250)	Thermo Fisher Scientific	A10040; RRID: AB_2534016
Donkey anti-Goat IgG, Alexa Fluor 647 (1:100)	Thermo Fisher Scientific	A32849; RRID: AB_2762840
Donkey anti-Mouse IgG, Alexa Fluor 546 (1:250)	Thermo Fisher Scientific	A-11003; RRID: AB_2534071
Alexa Fluor 488 Phalloidin (1:500)	Invitrogen	A12379
4,6-Diamidino-2-phenylindole (DAPI) (1:5000)	Thermo Fisher Scientific	D1306; RRID: AB_2629482
Alexa Fluor 488-conjugated phalloidin (1:1000)	Thermo Fisher Scientific	A12379
Anti-Digoxigenin-AP, Fab fragments (1:3000)	Sigma-Aldrich	11093274910; RRID: AB2734716
Chemicals, peptides, and recombinant proteins		
Paraformaldehyde	EMS	15710
Accutase	Innovative Cell Technologies	AT104
Thermolysin from geobacillus stearothermophilus (0.5 mg/mL)	Sigma-Aldrich	T7902
Medium 199 (HEPES buffered)	Sigma-Aldrich	M3769-10X1L
RNase-free PBS (137 mM NaCl, 2.7 mM KCl, 8 mM Na_2HPO_4, and 2 mM KH_2PO_4)	Thermo Fisher Scientific	AM9624
Triton X-100	Thermo Fisher Scientific	85111
recombinant RNase inhibitor	Clontech	2313B
dNTP Set (100 mM)	Thermo Fisher Scientific	10297018
Oligo-dT30 VN (2.5 μM, 5′-*AAGCAGTGGTATCAACGCAGAGTACT30VN*-3′)	IDT	https://www.idtdna.com/pages
AMPure Beads (60 mL)	Beckman Coulter	A63881
SUPERase·In™ RNase Inhibitor (20 U/μL)	Thermo Fisher Scientific	AM2696
SYTOX® Red dead cell stain	Thermo Fisher Scientific	S34859
Low melt agarose	BioRad	1613112
Plastic mold	VWR	15160-215
Blocking reagent	Sigma-Aldrich	11096176001
Tween-20	Sigma-Aldrich	P9416
Digoxigenin-11-UTP	Millipore Sigma	11209256910
Ribonucleoside triphosphate set	Millipore Sigma	11277057001
BM Purple	Sigma-Aldrich	11442074001
SSC (20X), RNase-free	Thermo Fisher Scientific	AM9770
CitiFluor CFM3 media	EMS	17979-30

REAGENT or RESOURCE	SOURCE	IDENTIFIER
FluorSave™ reagent	Calbiochem	345789-20ml
Secure-Seal™ spacer	Invitrogen	S24735
Secure-Seal™ hybridization sealing system	Electron Microscopy Sciences	70333-40
3M VHB Adhesive Seal Tabs	Electron Microscopy Sciences	70328-00
5-Ethynyl-2′-deoxyuridine	Thermo Fisher Scientific	A10044
Click-iT EdU Alexa Fluor 647 Imaging Kit	Thermo Fisher Scientific	C10340
Critical commercial assays		
CellsDirect™ One-Step qRT-PCR Kit	Thermo Fisher Scientific	11753100
SMARTScribe™ Reverse Transcriptase	Takara	639537
Hifi HotStart ReadyMix (2X)	Kapa Biosystems	KK2602
MEGAscript™ T7 Transcription Kit	ThermoFisher	AM1334
RNase Cocktail™ Enzyme Mix	Thermo Fisher Scientific	AM2288
Hybridization Chain Reaction v3.0	Molecular Instruments	https://www.molecularinstruments.com/hcr-v3
Deposited data		
Single cell RNA-sequencing data	This paper	GSE212831
Single cell RNA-sequencing data, web interface	This paper	gEAR
Single cell RNA-sequencing data (raw and normalized), cluster and trajectory annotation	This paper	Mendeley Data
Experimental models: Organisms/strains		
Fertilized chicken eggs	AA Laboratory Eggs Inc., Westminster, CA	N/A
Oligonucleotides		
HCR probe *RASD2*, Alexa Fluor® 488, XM_416293	Molecular Instruments	N/A
HCR probe *CABP1*, Alexa Fluor® 488, XM_004934386	Molecular Instruments	N/A
HCR probe *SMOC2*, Alexa Fluor® 488, XP_004935573.1	Molecular Instruments	N/A
HCR probe *SYT12*, Alexa Fluor® 546, NM_001199512	Molecular Instruments	N/A
HCR probe *KCNQ5*, Alexa Fluor® 546, XM_025148953	Molecular Instruments	N/A
HCR probe *CXCL14*, Alexa Fluor® 546, NM_204712.2	Molecular Instruments	N/A
HCR probe *TMC2*, Alexa Fluor® 546, NM_001039324	Molecular Instruments	N/A
Primers for generation of *in situ* hybridization probes	Supplemental information	Table S3
Software and algorithms		
FastQC tool	https://www.bioinformatics.babraham.ac.uk/projects/fastqc/	Version 0.11.6
STAR aligner	https://github.com/alexdobin/STAR/releases	STAR 2.7.8a
RSEM	http://deweylab.biostat.wisc.edu/rsem	RSEM v1.3.2

REAGENT or RESOURCE	SOURCE	IDENTIFIER
SingleCellExperiment - R package	https://www.bioconductor.org/packages/release/bioc/html/SingleCellExperiment.html	Version 1.6.0
scater - R package	https://bioconductor.org/packages/release/bioc/html/scater.html	Version 1.12.2
scran - R package	https://www.bioconductor.org/packages/release/bioc/html/scran.html	Version 1.12.1
SCnorm - R package	https://www.bioconductor.org/packages/release/bioc/html/SCnorm.html	Version 1.6.0
CellTrails - R package	https://www.bioconductor.org/packages/release/bioc/html/CellTrails.html	Version 1.2.0
ggplot2 - R package	https://ggplot2.tidyverse.org/	Version 3.3.0
gam - R package	https://cran.r-project.org/web/packages/gam/index.html	Version 1.2.0
yEd Graph Editor Software	https://www.yworks.com	Version 3.20
R Statistical Software	https://www.r-project.org	Version 3.6.2
Zen Blue and Zen Black	Zeiss	Version 14.0
Other		
SingleCellExperiment container with raw counts, normalized counts, log2 transformed normalized counts, state information, trajectories	Supplemental information Data S1	Data S1